International Journal of
Environmental Science
(IJES)

STEAM REFORMING OF METHANE OVER NICKEL CATALYST USING A ONE-DIMENSIONAL MODEL

RAKHI[1*], VIVIEN GÜNTHER[2], JANA RICHTER[1] AND FABIAN MAUSS[1]

IPRJB

International Journal of Environmental Sciences
ISSN 2519-5549 (online)
Vol.5, Issue 1, No.1. pp 1 - 32, 2022
www.iprjb.org

Steam reforming of methane over nickel catalyst using a one-dimensional model

Rakhi[1*], Vivien Günther[2], Jana Richter[1] and Fabian Mauss[1]
[1]BTU Cottbus-Senftenberg, Cottbus, 03046, Germany
[2]LOGE AB, Cottbus, 03044, Germany.*Corresponding author(s). E-mail(s): rakhi.rakhi@b-tu.de;
Contributing authors: vivien.guenther@logesoft.com; jana.richter@b-tu.de; maussf@b-tu.de;

ABSTRACT

Steam reforming of hydrocarbons is a well established chemical process which provides synthesis gas (H_2 and CO). These synthesis products can hence be converted to numerous valuable basic chemicals. For the industrial application of steam reforming, a detailed understanding of the process is a prerequisite. Models that capture the detailed homogeneous and heterogeneous reaction kinetics and the comprehensive transport processes as well as their interaction have the potential to optimize the catalytic process without expensive experimental campaigns.

In this paper, a detailed investigation has been done using a multi-step reaction mechanism for modeling steam reforming of methane over nickel-based catalyst using a one-dimensional (1D) model, LOGEcat [1]. The model is applicable to the simulation of all standard after-treatment catalytic processes of combustion exhaust gas along with other chemical processes involving heterogeneous catalysis, such as, the Sabatier process [27]. It is a 1D tool, thus is computationally cost effective and is based on a series of perfectly stirred reactors (PSR).

The model is used to perform the simulations for various reactor conditions in terms of temperature, pressure, flow rates and steam-to-carbon (S/C) ratio. Several chemical reaction terms, such as, selectivity, yield, conversion, and mole fraction have been shown with respect to the varied parameters and the results are compared with 2D simulations and experimental reference data. We report a very good agreement of the various profiles produced with 1D model as compared to the reference data.

Note that the main aim of this study is to check how far the 1D model can capture the basic chemistry for modeling steam reforming of methane over nickel-based catalysts. It is interesting to note that the cost effective reduced order model is capable to capture the physics and chemistry involved with a multi-step reaction mechanism showing the predictive capability of the model. This study forms the basis for further analysis towards the thermochemistry of the species to develop a kinetically consistent reaction mechanism.

Keywords: *Catalyst, One-dimensional modeling, Methane, Steam reforming*

1.0 INTRODUCTION

Steam reforming of hydrocarbons is a crucial chemical process [32,33,37] which provides synthesis gas (H_2 and CO). Due to the potential to reduce the cost of synthesis gas production and environmental concerns, steam as well as CO_2 reforming [15,23,7] of natural gas to synthesis gas have attracted much interest. The synthesis gas (in various compositions) plays a key role as a feedstock in many catalytic processes, for example, synthesis of methanol, oxosynthesis, and Fischer-Tropsch synthesis [24]. Furthermore, synthesis gas is a common hydrogen source for the manufacturing of ammonia [24]. The most prominent and widely used industrial steam reforming process is methane (natural gas) reforming. This is one of the most efficient technologies for hydrogen and synthesis gas production from fossil fuels in large scale facilities reaching yields close to the thermodynamic equilibrium [33,24,22]. Thus, conventional steam reformers deliver high concentrations of hydrogen at high fuel conversion rates [26]. However, this process is disadvantageous in small scale operation units because of the highly endothermic reactions and the requirement of efficient external energy supply. The molar steam-to-carbon (S/C) ratio generally surpasses 2.5 whereby the excess steam supports completion of the reactions and inhibits coke formation [43].

Coke deposition on catalysts and reactor pipe walls might lead to the blocking of reactor tubes as well as the physical disintegration of the catalyst structure [34,42,4,6,45] which makes noble metals, economically unsustainable due to their high prices, interesting as they are less prone to coke formation under oxidation and reforming conditions [31]. Nevertheless, in industrial applications, Ni based catalysts are preferred due to fast turnover rates, good availability and low cost, although limited by their higher tendency towards coke formation [17,16,8].

A deep understanding of the elementary steps involved in the reaction mechanism is necessary [10] in order to capture the involved physics and chemistry of the steam reforming process. A detailed literature review is provided in this direction. Reforming and oxidation of methane have been investigated using several techniques and different reaction mechanisms and corresponding kinetic models have been proposed that capture the gas reforming process properties under different conditions [47,35,5,20]. A catalytic sequence for reactions of CH_4 with CO_2 and H_2O on Ni/MgO catalysts has been postulated in [46] and a microkinetic model for steam reforming reactions over a $Ni/MgAl_2O_4$ catalyst has been proposed in [2] by reactions for CO_2 reforming of methane and deactivation by carbon formation. Earlier, a direct catalytic partial oxidation route has been followed [19,9], however, in later studies the overall conversion is assumed to happen in an indirect route by a two-step process [12,44,18,39]. The steps for steam reforming for the catalytic partial oxidation of methane over platinum and rhodium are published in [19,11,25,39,28]. Recently, a detailed mechanism for simultaneous modeling of partial oxidation and steam reforming over nickel catalyst have been discussed in [24]. [13] provides a review on catalytic partial oxidation of methane to synthesis gas with emphasis on reaction mechanism over transition metal catalysts. Further, steam reforming of methane accompanied by water-gas shift reactions on a $Ni/MgAl_2O_4$ catalyst is described by intrinsic rate equations derived from a Langmuir-Hinshelwood mechanism in [28].

All the investigations discussed above are either performed experimentally or by using 2D/3D tools therefore getting computationally expensive specially when the full reaction mechanism is

included. The increase in the computational cost is drastic with increasing number of species and alternatives need to be explored in order to capture the flow physics and chemistry at a reduced cost. Two strategies to reduce the computational cost come easily to mind, the first is to reduce the complexity of the chemical model and the second is to reduce the dimensionality from 2D/3D to 1D which is a time efficient alternative suitably applicable to catalyst simulations.

In this paper, the latter approach, reduction in dimensions is considered and a one-dimensional model, LOGEcat [1] which is discussed in the next section, has been elaborated to test the steam reforming of methane over nickel/alumina monoliths for different reactor inlet conditions. The results of the simulations that have been performed for several parameters, such as, temperature (T), pressure (P), steam-to-carbon (S/C) ratio and flow rate ($\dot{f}$), are compared with the data available in literature [24], for the 2D simulations as well as experiments.

Note that the focus of this paper is limited to recapture the existing chemistry to investigate the prediction capability of the 1D model which can, in future, be applied to chemistry training and device optimization. This study further forms the basis to investigate the reaction mechanism towards the kinetically limited conditions where the catalyst kinetics and internal transport are critical for the simulations.

2.0 MODEL DESCRIPTION

The 1D model LOGEcat [1] is used to carry out the simulations discussed in this paper. The model is based on the single-channel 1D catalyst model which is applicable to the simulation of all standard after-treatment catalytic processes of combustion exhaust gas, for example, three-way catalyst (TWC) [3], diesel oxidation catalysts (DOC), NO_x storage and reduction (NSR) catalysts and selective catalytic reduction (SCR) catalysts.

The model has been successfully applied and tested in previous studies [3,14,27]. The methanation of coke oven gas with nickel-based catalysts is investigated in [27] and the conversion effect using single and multiple channels model along with detailed kinetic model is presented in [3]. However, a detailed investigation of the steam reforming of methane over nickel in a generalised sense has not been considered in any of the previous studies. Here, we aim to analyze the given case in a general and detailed way in order to check the predictability of the model and to know how far the 1D model can capture the flow physics and the chemistry involved with it.

For the readability of this paper, we extend the discussion in the following sections to the modeling of the conservation and flow equations. The model can be used in single-channel mode and multi-channel mode. When running in multi-channel mode, pseudo 3D simulations are performed taking radial heat conduction between the channels into account. As this increases the computational cost, in this paper, only single-channel (discussed below) simulations are considered where radial heat transfer between the channels is not computed but the whole catalyst is represented using one channel. Note that a list of abbreviations and symbols used in this section or elsewhere is given in the end of the paper.

International Journal of Environmental Sciences
ISSN 2519-5549 (online)
Vol.5, Issue 1, No.1. pp 1 - 32, 2022
www.iprjb.org

2.1 Single Channel Model

The single channel as shown in Figure 1 is divided into a finite number of cells with Δx as their length and each cell is treated as a perfectly stirred reactor (PSR). The pressure gradient along with inhomogeneity of the mixture can be neglected as the diameter of the catalytic channel is small. A thin layer represented by a separate pore gas zone close to the wall is used to model the external diffusion.

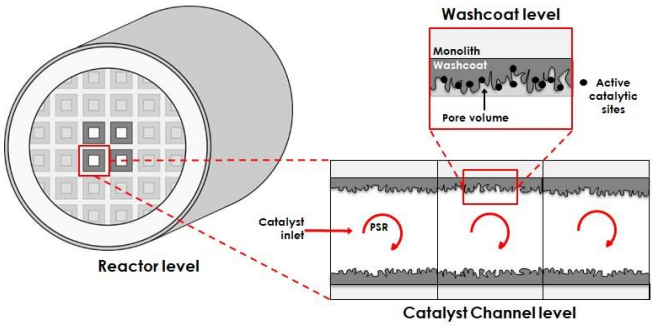

Figure 1: Schematic illustration of the modeling approach.

The model used to perform the simulations is a part of the LOGEsoft software suite [1] for chemical reaction calculations. The conservation equations given in the next section for gas species mass fraction, gas enthalpy, surface enthalpy, pore layer gas species mass fraction, and surface site fractions are solved in each PSR. These equations are solved for each time step. Additionally, the 1D Navier-Stokes equations for pressure as well as flow velocity are solved over all cells by an operator splitting method.

2.1.1 Conservation Equations

The bulk gas in each cell is modeled by a PSR with the constant pressure assumption during the time step Δt in the operator splitting loop. The mass transfer coefficient accounts for the species transport between bulk gas and pore volume layer. The conservation equation for bulk gas species mass fraction is given as,

$$\rho \frac{\partial Y_{i,g}}{\partial t} = \frac{(\rho v)_{in} A}{V_g}\left(Y_{i,in} - Y_{i,g}\right) + W_i \omega_{i,g} - \frac{P\Delta x}{V_g} W_i K_m k_{m,i}\left(C_{i,g} - C_{i,p}\right) + Y_{i,g} \frac{P\Delta x}{V_g} \sum_{j=1}^{N_g} W_j K_m k_{m,j}\left(C_{j,g} - C_{j,p}\right). \quad (1)$$

International Journal of Environmental Sciences
ISSN 2519-5549 (online)
Vol.5, Issue 1, No.1. pp 1 - 32, 2022
www.iprjb.org

The subscript *g* represents the bulk gas, *in* the inflow from the upstream cell and *p* gas in the pore layer. $Y_{i,g}$ is the mass fraction of species *i*, V_g is the gas volume in the current cell, $\omega_{i,g}$ is the species source term for gas phase reaction, K_m is the tunable parameter for the overall mass transfer, $k_{m,i}$ is the conservation mass transfer coefficient of species *i*, $C_{i,g}$ is the concentration of species *i* in the bulk gas, and $C_{i,p}$ is the concentration of species *i* in the pore layer. *P* is the geometric wetted perimeter of the channel. All the symbols are also summarised at the end of the paper. For more details, we refer the reader to [1].

The pore volume layer connects the gas phase to the surface through species pore diffusion. The conservation equation of the gas phase species is given as,

$$\begin{aligned}\rho_{p,l}\frac{\partial Y_{i,p,l}}{\partial t} = {} & \frac{P\Delta x}{V_{p,l}} W_i K_m k_{m,i}\left(C_{i,g} - C_{i,p,l}\right)\big|_{l=1} + W_i\omega_{i,p,l} \\ & + W_i K_e \sum_{m=1}^{N_{surf}} \frac{A_m}{V_{p,l}}\omega_{i,m} + D_i \frac{C_{i,p,l} - C_{i,p,l+1}}{W_{l+1,l}}\frac{A_m}{V_{p,l}} \\ & - Y_{i,p,l}\sum_{j=1}^{N_g}\left[\frac{P\Delta x}{V_{p,l}} K_m k_{m,j} W_j\left(C_{j,g} - C_{j,p,l}\right)\big|_{l=1}\right. \\ & \left. + W_j K_e \sum_{m=1}^{N_{surf}} \frac{A_m}{V_{p,l}}\omega_{j,m} + D_i \frac{C_{j,p,l} - C_{j,p,l+1}}{W_{l+1,l}}\frac{A_m}{V_{p,l}}\right]. \end{aligned} \quad (2$$

In the above equation, $V_{p,l}$ is the gas volume of the pore volume layer of washcoat layer *l* in the current cell, $\omega_{i,p,l}$ is the species source term for gas phase reactions in the pore layer of washcoat *l*, N_{surf} is the number of different surface materials present in the catalytic converter (usually 1) and A_m is the catalytic surface area in the current cell. K_e is the tuning parameter for the overall reaction efficiency and the parameter D_i accounts for an additional term for diffusion through multiple washcoat layers which is appropriate diffusion coefficient for species *i*, the subscript *l* is the current washcoat layer, $W_{l+1,l}$ is the radial distance through the washcoat calculated as $(W_{l+1}-W_l)/2$ for diffusion between washcoat layer *l* and *l*+1. Note that the source term for bulk gas species transport to the washcoat is only used for the first washcoat layer denoted as $|_{l=1}$.

Next, the conservation equation for surface species site fraction is given as,

$$\frac{\partial\theta_{i,n}}{\partial t} = \sigma_{i,n}K_e\frac{\omega_{i,n}}{\tau_n}. \quad (3$$

Here, $\theta_{i,n}$ indicates the site fraction of species *i* at site *n*, τ_n is the site density, $\omega_{i,n}$ is the species source term from reactions at site *n* and $\sigma_{i,n}$ is the site occupancy number of species *i* at site *n*.

The heat transport by convection and molecular transport is taken into account by the bulk energy (specific enthalpy) and the conservation equation is given as,

$$\frac{\partial h_g}{\partial t} = -K_h h_T \frac{P\Delta x}{m_g}\left(T_g - T_w\right) + \frac{(\rho v)_{in} A}{m_g}\left(h_{in} - h_g\right) + \frac{P\Delta x}{m_g}\sum_{j=1}^{N_g} W_j K_m k_{m,j}\left(C_{j,g} - C_{j,p}\right)\left(h_g - h_{j,g\leftrightarrow p}\right). \quad (4$$

In the above equation, h_g is the bulk gas specific enthalpy, K_h is the tunable parameter for the overall heat transfer, h_T is the convective heat transfer coefficient between bulk gas and surface, T_g is the bulk gas temperature, T_w the pore layer temperature, h_{in} is the specific enthalpy of the gas from the upstream cell and $h_{j,g\leftrightarrow p}$ the specific enthalpy of species j transported between the bulk gas and the pore layer. The bulk gas enthalpy is used in case of the species being transported from the bulk gas whereas, pore layer enthalpy is used if it is transported to the bulk gas.

The pressure is assumed constant in the pore layer, the pore layer temperature is assumed to be homogeneous for the substrate as well as for the gas and the kinetic energy due to gas movement is neglected. With all these assumptions, the conservation equation for the surface enthalpy is given as,

$$\begin{aligned}\left(\rho_s V_s c_{p,s} + \rho_p V_p c_{p,p}\right)\frac{\partial T_w}{\partial t} &= V_s \frac{\partial}{\partial x}\left(k_s \frac{\partial T_w}{\partial x}\right) + K_h h_T P\Delta x\left(T_g - T_w\right) \\ &- \sum_{j=1}^{N_{g,p}} W_j P\Delta x\, K_m k_{m,j}\left(C_{j,g} - C_{j,p}\right)\left(h_{j,p} - h_{j,g\leftrightarrow p}\right) \\ &- \sum_{j=1}^{N_{g,p}} W_j \left[h_{j,p} V_p K_e \omega_{j,p} + h_{j,p} K_e \sum_{m=1}^{N_m} A_m \omega_{j,m}\right] \\ &- K_e \sum_{m=1}^{N_m}\sum_{j=1}^{N_{s,m}} h_{j,m} W_j A_m \omega_{j,m} \\ &+ \frac{k_{s,l+1}\left(\frac{\partial T_{w,l+1}}{\partial w_{l+1,l-1}}\right) - k_{s,l-1}\left(\frac{\partial T_{w,l-1}}{\partial w_{l+1,l-1}}\right)}{w_l},\end{aligned} \quad (5$$

where, V_s is the volume of the solid wall material (washcoat and substrate) in the current cell, $c_{p,s}$ is the specific heat capacity of the solid material at constant pressure and $c_{p,p}$ is the specific heat capacity in the pore volume layer at constant pressure. Therefore, the above equation accounts for heat conduction along the channel, heat convection/ diffusion to the bulk gas, molecular heat transport as well as heat released by reactions. $k_{s,l}$ is the thermal conductivity of washcoat layer l. For single washcoat, pore diffusion is mimicked by the tunable parameter K_e. The washcoat diffusion for the surface temperature is also included in case of multiple washcoats. In addition, heat flow term is used to account for heat losses through the material and the catalyst at the periphery of the substrate.

The mass and heat transfer coefficients, $k_{m,i}$ and h_T, used in the conservation equations are calculated from the Sherwood and Nusselt numbers [21]. For simultaneously developing, concentration and thermal boundary layer flow, the correlations for Sherwood and Nusselt numbers are utilized as [30],

$$h_i(x) = \begin{cases} \frac{0.35}{Sc_i^{1/6}} \sqrt{\frac{(\frac{d_h}{4})^2 v}{xD_i}}, & 0 < x < \frac{(\frac{d_h}{4})^2 v}{D_i} (\frac{1}{Sc_i})^{1/3} (\frac{1.4}{Sh_{T,\infty}})^2 \\ Sh_{T,\infty}, & x \geq \frac{(\frac{d_h}{4})^2 v}{D_i} (\frac{1}{Sc_i})^{1/3} (\frac{1.4}{Sh_{T,\infty}})^2, \end{cases} \quad (6$$

$$\begin{cases} \frac{0.35}{Pr^{1/6}} \sqrt{\frac{(\frac{d_h}{4})^2 v}{xD_T}}, & 0 < x < \frac{(\frac{d_h}{4})^2 v}{D_T} (\frac{1}{Pr})^{1/3} (\frac{1.4}{Nu_{T,\infty}})^2 \\ Nu_{T,\infty}, & x \geq \frac{(\frac{d_h}{4})^2 v}{D_T} (\frac{1}{Pr})^{1/3} (\frac{1.4}{Nu_{T,\infty}})^2. \end{cases} \quad (7$$

Here, d_h is the hydraulic diameter of the channel, D_i is the species diffusion coefficient for species i, D_T is the thermal diffusion coefficient and v is the fluid velocity along the channel. $Sh_{T,\infty}$ and $Nu_{T,\infty}$ are the asymptotic Sherwood and Nusselt numbers, respectively, for constant flux boundary conditions and their values are taken from [36]. Further, the Schmidt number for species i, Sc_i and the Prandtl number, Pr are given as,

$$Sc_i = \frac{\mu_i}{\rho D_i}, \quad (8$$

$$Pr = \frac{c_p \mu}{k_g}, \quad (9$$

where, μ_i is the dynamic viscosity. c_p is the heat capacity at constant pressure and k_g is the thermal conductivity of the gas.

2.1.2 Flow Equations

The conservation equations, with the assumption that the flow is in steady state, are given below,

$$\frac{\partial(\rho v)}{\partial x} = -\frac{A_{w,G}}{m_g}\sum_{i=1}^{N_g} W_i\, k_{m,i}(C_{i,g} - C_{i,p}), \qquad (10$$

$$\frac{\partial(\rho v^2)}{\partial x} + \frac{\partial p}{\partial x} = -\frac{f_F}{2}(\rho v)|v|\frac{p}{A}, \qquad (11$$

as the mass and momentum equations, respectively. In the above equations, A is the cross-sectional channel area and the friction factor, f_F for laminar and fully developed flow is given as,

$$f_F = \frac{16}{Re} = \frac{16\mu}{\rho v d_h}. \qquad (12$$

For more details related to the derivations for the equations and the model, we refer the reader to [1].

3.0 SURFACE REACTION MECHANISM

The conversion of methane and steam into a mixture of hydrogen, carbon monoxide and carbon dioxide can be considered as a combination of several reactions. This section covers the detailed surface reaction mechanism involved in our investigation along with the thermodynamic consistency.

Note that we have used the reaction mechanism from [24,38] to model reforming of methane on nickel which contains 7 gas phase species and 13 surface species in total. The reaction mechanism consists of 42 reactions and these reactions are summarized in Table 1 along with their rate expressions [24]. The reaction mechanism indicates that adsorbed carbon species (C, CH, CH_2, CH_3) formed from activated methane reacts with adsorbed atomic oxygen O(s), formed from the adsorption of oxygen or from the decomposition of water and CO_2, and produce carbon oxide. The mechanism also comprises the reactions of partial oxidation and steam reforming of methane and is based on the key reaction intermediate - adsorbed atomic oxygen O(s). The sticking coefficients (s.c.) are used as kinetic data for the adsorption of reactants and

products (H_2, O_2, CH_4, H_2O, CO, CO_2) given in the reaction mechanism. For the details of the reaction mechanism, we refer the reader to [24].

The equilibrium of a chemical reaction is given as,

$$\sum_i v'_{ir} A_i \underset{k_{b,r}}{\overset{k_{f,r}}{\rightleftarrows}} \sum_i v''_{ir} A_i, \qquad (13$$

and is defined by the thermodynamic properties of the participating species *i*. The chemical source terms due to catalytic reactions are modeled by elementary-step based reaction mechanisms [41]. In the present study, the homogeneous gas-phase reactions can be neglected. The forward rate constants, $k_{f,r}$, for the reactions *r* are generally assumed to have the following Arrhenius temperature dependence (for gas-phase as well as surface species),

$$k_{f,r} = A_r T^{\beta_r} \exp\left(\frac{-E_r}{R_c T}\right), \qquad (14$$

where, A_r is the pre-exponential factor, β_r is the temperature exponent and E_r is the activation energy. T is the gas temperature and R_c is the gas constant in units consistent with activation energy. The forward rate is modified for the reactions involving coverage parameters and sticking coefficients, discussed below [1].

The thermodynamic data associated with each species in a reaction are used to calculate the equilibrium constant and reverse rate coefficients for a reaction. In the thermal systems, the reverse rate constants, $k_{b,r}$, are related to the forward rate constants through the equilibrium constants given as,

$$k_{b,r} = \frac{k_{f,r}}{K_{c,r}}. \qquad (15$$

$K_{c,r}$ is the equilibrium constant given in concentration units which considers the surface state as well as the gas state in case of reactions involving surface species as,

International Journal of Environmental Sciences
ISSN 2519-5549 (online)
Vol.5, Issue 1, No.1. pp 1 - 32, 2022
www.iprjb.org

$$K_{c,r} = K_{p,r}\left(\frac{P_{atm}}{R_0 T}\right)^{\sum_{i=1}^{Sg} \nu_{i,r}} \prod_{n=N_{surf}^{f}}^{N_{surf}^{l}} \left(\Gamma_n^0\right)^{\sum_{i=K_{surf}^{f}(n)}^{K_{surf}^{l}(n)} \nu_{i,r}} \prod_{i=K_{surf}^{f}(n)}^{K_{surf}^{l}(n)} \sigma_i^{-\nu_{i,r}}, \quad (16$$

where, P_{atm} denotes a pressure of 1 atm, R_0 is the universal gas constant, $\nu_{i,r}$ represents the stoichiometric coefficients for reaction r and species i, Γ_n^0 is the standard-state surface site density of site type n and σ_i is the number of sites that the surface species occupies. The sum in the first exponent runs only over the gas-phase species, whereas the sum in the second exponent runs only over surface species in surface phase n.

The equilibrium constants, $K_{p,r}$, in pressure units has the same form as for gas-phase reactions given as,

$$K_{p,r} = \exp\left(\frac{\Delta S_r^0}{R_0} - \frac{\Delta H_r^0}{R_0 T}\right), \quad (17$$

with Δ as the change that occurs in passing completely from reactants to products in the r^{th} reaction and S and H are the symbols used for entropy and enthalpy, respectively (superscript ^{0} denotes the standard-state) which are calculated using thermodynamic data as,

$$\frac{\Delta S_r^0}{R_0} = \sum_{i=1}^{S} \nu_{i,r} \frac{S_i^0}{R_0}, \quad (18$$

$$\frac{\Delta H_r^0}{R_0 T} = \sum_{i=1}^{S} \nu_{i,r} \frac{H_i^0}{R_0 T}. \quad (19$$

To summarize, equation (14) is used to calculate the rate constants in case of an irreversible reaction which means that the rate coefficients (A_r, β_r and E_r) are specified for all the reactions in the input file. Whereas, in case of a reversible reaction, forward rate constant is calculated using

equation (14) and reverse rate calculated using equation (15) which also uses the equilibrium rate constant obtained from thermodynamic data.

Nonetheless, the forward and the reverse reactions are defined separately with their own rate laws due to missing thermodynamic data for the problems encountered in setting up a reaction mechanism. Indeed, it is difficult to define thermodynamic data for intermediate surface species. The thermodynamic consistency is ensured in a sense that the thermodynamic equilibrium of the participating gas-phase species is matched for a range of temperatures, while writing all reversible reactions as pairs of independent forward and backward reactions. The thermodynamic data of the intermediate species is, therefore not needed for the evaluation of the reaction rates [24]. We do not aim to cover further details in this section and hence leave this to the reader's interest. Note that the reaction mechanism and the thermodynamic data for all the species used in the present study are taken from [24,38].

3.1 Surface-coverage Modification of Rate Expression

Arrhenius expression for the rate constant, i.e., equation (14), is modified by the coverage (concentration) of some surface or bulk species (optional coverage parameters to be specified for species *i* and reaction *r* as done for R12, R36, R37 and R40 in Table 1). The rate constant for the forward reaction is modified as,

$$k_{f,r} = A_r T^{\beta_r} \exp\left(\frac{-E_r}{R_0 T}\right) \prod_{i=K^f_{surf}\left(N^f_{surf}\right)}^{K^l_{surf}\left(N^l_{surf}\right)} 10^{\eta_{i,r}[Z_{i,n}]} \left[Z_{i,n}\right]^{\mu_{i,r}} \exp\left(\frac{-\varepsilon_{i,r}[Z_{i,n}]}{R_0 T}\right) \prod_{i=K^f_{bulk}\left(N^f_{bulk}\right)}^{K^l_{bulk}\left(N^l_{bulk}\right)} 10^{\eta_{i,r}[a_{i,n}]} \left[a_{i,n}\right]^{\mu_{i,r}} \exp\left(\frac{-\varepsilon_{i,r}[a_{i,n}]}{R_0 T}\right). \quad (20$$

$\eta_{i,r}$, $\mu_{i,r}$ and $\varepsilon_{i,r}$ are coverage parameters. $Z_{i,n}$ is the surface site fractions for surface species and $a_{i,n}$ is the bulk activity for bulk species. The reverse and equilibrium rate constants are calculated using equations (14) and (16). With the modified rate constant, the net pre-exponential factor and the activation energy are the function of coverage as,

$$logA = logA_r + \sum_{i=K^f_{surf}\left(N^f_{surf}\right)}^{K^l_{surf}\left(N^l_{surf}\right)} \eta_{i,r}\left[Z_{i,n}\right] + \sum_{i=K^f_{bulk}\left(N^f_{bulk}\right)}^{K^l_{bulk}\left(N^l_{bulk}\right)} \eta_{i,r}\left[a_{i,n}\right], \quad (21$$

$$E = E_r + \sum_{i=K_{surf}^{f}\left(N_{surf}^{f}\right)}^{K_{surf}^{l}\left(N_{surf}^{l}\right)} \varepsilon_{i,r}\left[Z_{i,n}\right] + \sum_{i=K_{bulk}^{f}\left(N_{bulk}^{f}\right)}^{K_{bulk}^{l}\left(N_{bulk}^{l}\right)} \varepsilon_{i,r}\left[a_{i,n}\right]. \quad (22$$

Table 1: Thermodynamically consistent surface reaction mechanism [24]. A_r is the pre-exponential factor, E_r is the activation energy and β_r is the temperature exponent. s.c. indicates the sticking coefficients.

	Reaction	A_r (cm,mol,s)		E_r (kJ/mol)	$\beta_r(-)$
R1	$H_2 + 2Ni(s) \rightarrow 2H(s)$	1.000×10^{-02}	(s.c.)	0.00	0.0
R2	$2H(s) \rightarrow H_2 + 2Ni(s)$	$2.545\times10^{+19}$		81.21	0.0
R3	$O_2 + 2Ni(s) \rightarrow 2O(s)$	1.000×10^{-02}	(s.c.)	0.00	0.0
R4	$2O(s) \rightarrow O_2 + 2Ni(s)$	$4.283\times10^{+23}$		474.95	0.0
R5	$CH_4 + Ni(s) \rightarrow CH_4(s)$	8.000×10^{-03}	(s.c.)	0.00	0.0
R6	$CH_4(s) \rightarrow CH_4 + Ni(s)$	$8.705\times10^{+15}$		37.55	0.0
R7	$H_2O + Ni(s) \rightarrow H_2O(s)$	1.000×10^{-01}	(s.c.)	0.00	0.0
R8	$H_2O(s) \rightarrow H_2O + Ni(s)$	$3.732\times10^{+12}$		60.79	0.0
R9	$CO_2 + Ni(s) \rightarrow CO_2(s)$	1.000×10^{-05}	(s.c.)	0.00	0.0
R10	$CO_2(s) \rightarrow CO_2 + Ni(s)$	$6.447\times10^{+07}$		25.98	0.0
R11	$CO + Ni(s) \rightarrow CO(s)$	5.000×10^{-01}	(s.c.)	0.00	0.0
R12	$CO(s) \rightarrow CO + Ni(s)$	$3.563\times10^{+11}$		111.27	0.0
	COV /CO(s)	$0.000\times10^{+00}$		-50.0	0.0
R13	$CH_4(s) + Ni(s) \rightarrow CH_3(s) + H(s)$	$3.700\times10^{+21}$		57.7	0.0
R14	$CH_3(s) + H(s) \rightarrow CH_4(s) + Ni(s)$	$6.034\times10^{+21}$		61.58	0.0
R15	$CH_3(s) + Ni(s) \rightarrow CH_2(s) + H(s)$	$3.700\times10^{+24}$		100.0	0.0
R16	$CH_2(s) + H(s) \rightarrow CH_3(s) + Ni(s)$	$1.293\times10^{+23}$		55.33	0.0
R17	$CH_2(s) + Ni(s) \rightarrow CH(s) + H(s)$	$3.700\times10^{+24}$		97.10	0.0
R18	$CH(s) + H(s) \rightarrow CH_2(s) + Ni(s)$	$4.089\times10^{+24}$		79.18	0.0
R19	$CH(s) + Ni(s) \rightarrow C(s) + H(s)$	$3.700\times10^{+21}$		18.8	0.0
R20	$C(s) + H(s) \rightarrow CH(s) + Ni(s)$	$4.562\times10^{+22}$		161.11	0.0
R21	$CH_4(s) + O(s) \rightarrow CH_3(s) + OH(s)$	$1.700\times10^{+24}$		88.3	0.0
R22	$CH_3(s) + OH(s) \rightarrow CH_4(s) + O(s)$	$9.876\times10^{+22}$		30.37	0.0
R23	$CH_3(s) + O(s) \rightarrow CH_2(s) + OH(s)$	$3.700\times10^{+24}$		130.1	0.0
R24	$CH_2(s) + OH(s) \rightarrow CH_3(s) + O(s)$	$4.607\times10^{+21}$		23.62	0.0
R25	$CH_2(s) + O(s) \rightarrow CH(s) + OH(s)$	$3.700\times10^{+24}$		126.8	0.0
R26	$CH(s) + OH(s) \rightarrow CH_2(s) + O(s)$	$1.457\times10^{+23}$		47.07	0.0
R27	$CH(s) + O(s) \rightarrow C(s) + OH(s)$	$3.700\times10^{+21}$		48.1	0.0
R28	$C(s) + OH(s) \rightarrow CH(s) + O(s)$	$1.625\times10^{+21}$		128.61	0.0
R29	$H(s) + O(s) \rightarrow OH(s) + Ni(s)$	$5.000\times10^{+22}$		97.9	0.0
R30	$OH(s) + Ni(s) \rightarrow H(s) + O(s)$	$1.781\times10^{+21}$		36.09	0.0

R31	$H(s) + OH(s) \rightarrow H_2O(s) + Ni(s)$	$3.000\times10^{+20}$	42.7	0.0
R32	$H_2O(s) + Ni(s) \rightarrow H(s) + OH(s)$	$2.271\times10^{+21}$	91.76	0.0
R33	$OH(s) + OH(s) \rightarrow H_2O(s) + O(s)$	$3.000\times10^{+21}$	100.0	0.0
R34	$H_2O(s) + O(s) \rightarrow OH(s) + OH(s)$	$6.373\times10^{+23}$	210.86	0.0
R35	$C(s) + O(s) \rightarrow CO(s) + Ni(s)$	$5.200\times10^{+23}$	148.1	0.0
R36	$CO(s) + Ni(s) \rightarrow C(s) + O(s)$	$1.354\times10^{+22}$	116.12	-3.0
	COV /CO(s)	$0.000\times10^{+00}$	-50.0	0.0
R37	$CO(s) + O(s) \rightarrow CO_2(s) + Ni(s)$	$2.000\times10^{+19}$	123.6	0.0
	COV /CO(s)	$0.000\times10^{+00}$	-50.0	0.0
R38	$CO_2(s) + Ni(s) \rightarrow CO(s) + O(s)$	$4.653\times10^{+23}$	89.32	-1.0
R39	$CO(s) + H(s) \rightarrow HCO(s) + Ni(s)$	$4.019\times10^{+20}$	132.23	-1.0
R40	$HCO(s) + Ni(s) \rightarrow CO(s) + H(s)$	$3.700\times10^{+21}$	0.0	0.0
	COV /CO(s)	$0.000\times10^{+00}$	50.0	0.0
R41	$HCO(s) + Ni(s) \rightarrow CH(s) + O(s)$	$3.700\times10^{+24}$	95.8	-3.0
R42	$CH(s) + O(s) \rightarrow HCO(s) + Ni(s)$	$4.604\times10^{+20}$	109.97	0.0

3.2 Sticking Coefficients

For some surface reaction mechanisms, the surface reaction rate constant is specified in terms of a ”sticking coefficient” (probability), rather than an actual reaction (see R1, R3, R5, R7, R9 and R11 in Table 1). In such cases, the unitless sticking coefficients’ functional form has an ”Arrhenius-like” form which is given as,

$$\gamma_r = \min[1, a_r T^{b_r} \exp\left(\frac{r}{R_c T}\right)], \qquad (23$$

γ_r, a_r and b_r are unitless and r has units compatible with R_cT (the real gas constant used for reaction activation energies multiplied by temperature). The collision frequency of the gas species with the solid surface is used for the conversion of a sticking coefficient, γ_r, to the usual mass-action kinetic rate constant given as,

$$k_{f,r} = \left(\frac{\gamma_r}{1 - \frac{\gamma_r}{2}}\right) \frac{\prod_{i=1} \sigma_i^{\nu'_{r,i}}}{(\Gamma_{tot})^m} \sqrt{\frac{R_0 T}{2\pi W_k}}. \qquad (24$$

R_0 is the universal gas constant, W_k is the molecular weight of the gas-phase species, Γ_{tot} is the total surface site concentration summed over all surface phases (number of moles of surface sites per unit area), m is the sum of all the stoichiometric coefficients of reactants that are surface

species, σ_i is the number of sites that the surface species occupies and $v_{r,i}$ is the reaction order for that species. The reverse and equilibrium rate constants are calculated as explained in the previous section.

With the above modifications of the rate constant, the net pre-exponential factor is given as,

$$A_r = \frac{\prod_{i=1} \sigma_i^{\nu'_{r,i}}}{(\Gamma_{tot})^m} \sqrt{\frac{R_0}{2\pi W_k}}. \qquad (25$$

4.0 SIMULATION SET-UP

The simulation set-up used for the present study follows from [24]. The geometric data and catalyst parameters to perform the simulations are summarized in Table 2. The investigation is extended for different reactor conditions in terms of parameters, such as, temperature, S/C ratio, flow rate and pressure summarised in Table 3. Analysis is done for four different temperatures, T=920,1020,1120, and 1220 K while keeping all other parameters (S/C, $\dot{f}$ and P) constant. Similarly, the S/C ratio is varied as S/C=1.9,2.77, and 3.67, flow rate as $\dot{f}$=296,593 and 1186 mL/min and pressure as P=1,10 and 100 atm with other parameters fixed.

We have considered a single channel and it is uniformly divided into 25 cells. One layer of washcoat is used for the simulations. The overall heat transfer efficiency factor, mass transfer efficiency factor and efficiency factors for surface chemistry are taken as unity. The surface site density, τ for Ni is 2.6×10^{-5} mol/m^2 [33]. The surface area per catalyst length is used as 6.9×10^{-2} m^2/m. 75% Argon dilution is used.

Table 2: The geometric data and catalyst parameters used to carry out the simulations.

Catalyst channel geometry	Quadratic	
Number of cells per channel (lengthwise)	25	
Channel density	640	cpsi
Length	3.0×10^{-2}	m
Hydraulic diameter	1.13×10^{-3}	m
Catalyst geometry	Circular	
Catalyst radius	7.5×10^{-3}	m
Washcoat thermal conductivity	250	W/m/K
Washcoat thickness	5.0×10^{-5}	m
Washcoat porosity	0.8	

Table 3: Summary of the simulation cases performed for the set-up considered from [24]. T is the temperature in K, S/C is the inlet steam-to-carbon ratio (C/S as carbon to steam), $\dot{f}$ is the flow rate in mL/min, P is the pressure in Pa and the inlet composition of the species is given in mole fraction.

Case	T [K]	S/C (C/S)	$\dot{f}$ [mL/min]	P [Pa]	CH_4	H_2O	Ar
C1	922.94	2.77 (0.36)	593	1.01325×10^5	0.0663	0.1837	0.75
C2	1019.05	2.77 (0.36)	593	1.01325×10^5	0.0663	0.1837	0.75
C3	1120.27	2.77 (0.36)	593	1.01325×10^5	0.0663	0.1837	0.75
C4	1214.93	2.77 (0.36)	593	1.01325×10^5	0.0663	0.1837	0.75
C5	1020	1.90 (0.53)	593	1.01325×10^5	0.0862	0.1638	0.75
C6	1020	2.77 (0.36)	593	1.01325×10^5	0.0663	0.1837	0.75
C7	1020	3.67 (0.27)	593	1.01325×10^5	0.0535	0.1965	0.75
C8	1020	2.77 (0.36)	296	1.01325×10^5	0.0663	0.1837	0.75
C9	1020	2.77 (0.36)	593	1.01325×10^5	0.0663	0.1837	0.75
C10	1020	2.77 (0.36)	1186	1.01325×10^5	0.0663	0.1837	0.75
C11	[600-1300]	3.00 (0.34)	593	1.01325×10^5	0.25	0.75	0.00
C12	[600-1300]	3.00 (0.34)	593	1.01325×10^6	0.25	0.75	0.00
C13	[600-1300]	3.00 (0.34)	593	1.01325×10^7	0.25	0.75	0.00

5.0 RESULTS

The model explained in the previous sections uses the above set-up to perform the simulations of steam reforming of methane over a nickel catalyst and all the kinetic parameters are taken from [24]. Some of the important terms encountered in chemical reaction engineering are conversion, selectivity, yield and mole fraction which are discussed in this section. It is important to check these quantities to see if the system is consistent. The variation of these quantities is shown with different parameters, for example, temperature, pressure, S/C ratio and flow rate.

The conversion describes the ratio of how much of a reactant has reacted and lies between zero and one. The yield shows the formation of a desired product and it also falls in between zero and one. The selectivity defines the ratio of the desired product to the undesired products. The mole fraction of species *i* is the fraction of moles it occupies relative to the total number of moles in the mixture and the sum of mole fractions will necessarily become unity. The formulas for these quantities are given where they are first discussed in the section.

We have investigated several parameters in complete detail in order to re-confirm the basic chemistry and to check the predictability of the model before capturing the new results. The study will apply the model to more complex investigations in future. Note that the preliminary results with the set-up used here have been discussed in [29], however, in this paper a much more detailed analysis is presented.

International Journal of Environmental Sciences
ISSN 2519-5549 (online)
Vol.5, Issue 1, No.1. pp 1 - 32, 2022
www.iprjb.org

5.1 Variation of Temperature

In this section, we present the simulation results for 4 different temperatures as T=920,1020,1120, and 1220 K. All the other physical and numerical parameters are kept constant. The simulations are performed for fixed S/C ratio as 2.77, pressure as 1 atm, flow rate as 593 mL/min and 75% Argon dilution.

The conversion of methane and water as a function of temperature along with the reference data is shown in Figure 2. The equilibrium calculations for the reference data are also given in the figure. The conversion X for species *i* is defined as the ratio of the total molar rate of the consumption of species *i* to the molar flow rate of the species *i* in the feed which is calculated as, $X_i = (y_{i,in}-y_{i,out})/y_{i,in}$ where y_i is the mass fraction of species *i*. The 1D simulation results using LOGEcat model are in very good agreement with the experimental and simulation results from [24]. It is observed that the thermodynamic equilibrium is attained at the higher temperatures. However, at higher temperatures the simulation results, both from LOGEcat model as well as 2D reference data, deviate from the experimental data.

Figure 3 shows the CO selectivity variation with temperature in methane steam reforming for other parameters fixed along with the reference simulation and experimental data. The selectivity, *S* is defined as the ratio of the total molar rate of production of desired product to the total molar rate of production of undesired product and for CO is calculated as, $S_{CO} = x_{CO}/(x_{CO} + x_{CO2} + x_{CH4})$ where x is the mole fraction of the species given in subscript. We observe a very good agreement for the 1D LOGEcat model results with [24].

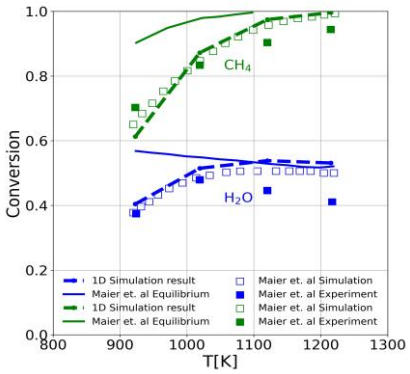

Figure 2: Methane and water conversion as a function of temperature while keeping all the other parameters fixed as S/C=2.77, P=1 atm, $\dot{f}$=593 mL/min and 75% Argon dilution along with the reference data.

International Journal of Environmental Sciences
ISSN 2519-5549 (online)
Vol.5, Issue 1, No.1. pp 1 - 32, 2022
www.iprjb.org

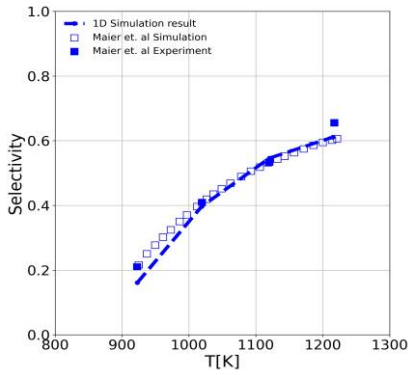

Figure 3: CO Selectivity variation with temperature in methane steam reforming while keeping all the other parameters fixed as S/C=2.77, P=1 atm, $\dot{f}$=593 mL/min and 75% Argon dilution along with the reference data.

Figure 4 illustrates the H_2/CO ratio variation with the temperature in methane steam reforming for fixed S/C ratio, pressure and flow rate along with the reference results. As explained in [24], the over-prediction of the H_2/CO ratio in comparison to the experimental measurements at the given S/C ratio (=2.77) might be due to the underestimation of water-gas shift reaction at low temperature in the 2D as well as 1D models. The H_2/CO ratio for simulations, Maier's 2D simulations as well as results from the 1D model, is higher compared to the equilibrium calculation at temperature ≤1000 K. The 1D results lie in between the experimental and simulation reference results from [24]. Nonetheless, it is worth noticing that the 1D model captures these quantities, qualitatively as well as quantitatively very well.

Further, in Figure 5 and 6 the variation of concentration for reactants and products along with the axial distance of the reactor is shown. The simulation results are displayed for only one temperature, T=920 K. These figures illustrate that the reactants (Figure 5), methane and water, are being used in the first few seconds, i.e., within 2s and then the thermal equilibrium is reached.

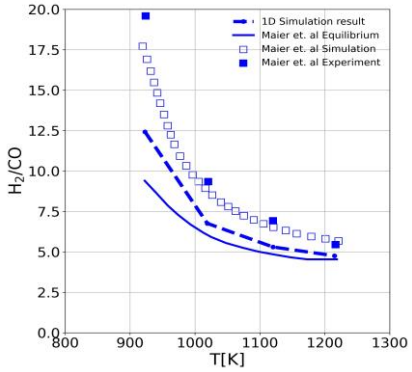

Figure 4: H_2/CO ratio variation with temperature in methane steam reforming while keeping all the other parameters fixed as S/C=2.77, P=1 atm, $\dot{f}$=593 mL/min and 75% Argon dilution along with the reference data.

International Journal of Environmental Sciences
ISSN 2519-5549 (online)
Vol.5, Issue 1, No.1. pp 1 - 32, 2022
www.iprjb.org

No change in the concentration can be observed after 2s but the simulations do run a little longer in order to make sure that steady state is reached. Similarly, the formation of products (Figure 6), H_2, CO, CO_2, also takes place within the first few seconds and then it ceases. This behaviour was expected as the endothermic reactions are dominant on the catalytic surface in the initial phase which cause the major changes in concentration of different species only in the beginning and then the system attains thermal equilibrium.

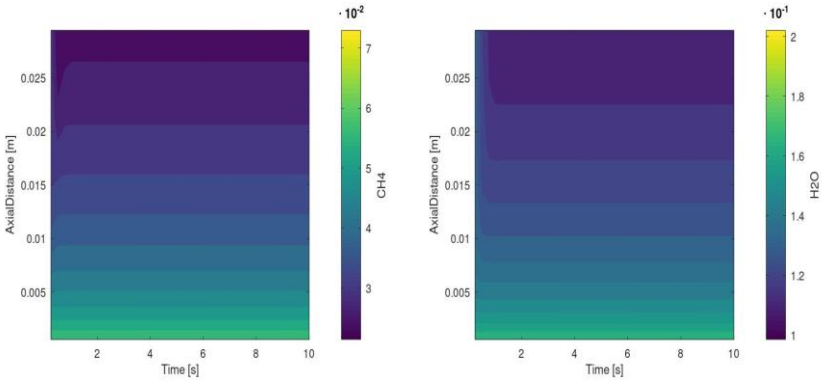

Figure 5: (a) Methane and (b) water concentration along the reactor for T=920 K.

International Journal of Environmental Sciences
ISSN 2519-5549 (online)
Vol.5, Issue 1, No.1. pp 1 - 32, 2022
www.iprjb.org

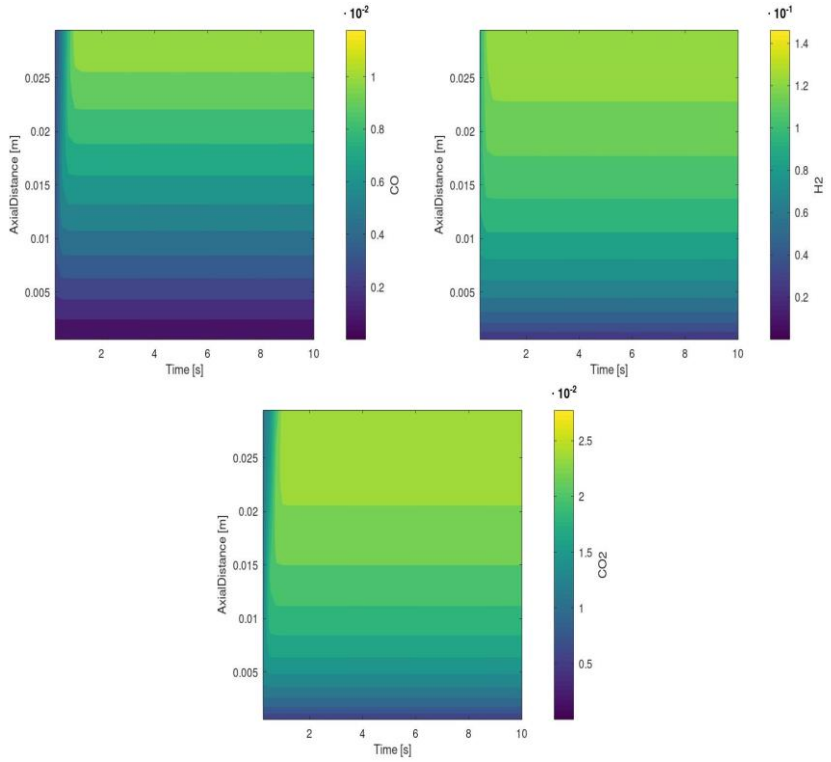

Figure 6: (a) CO, (b) H_2 and (c) CO_2 concentration along the reactor for T=920 K.

In Figure 7, the methane and water conversion is shown as a function of temperature for fixed S/C ratio (S/C=3), pressure and flow rate along with the reference data. The figure captures the conversion behaviour for a wide range of temperatures, Tϵ[600,1300] K in order to check the predictability of the 1D model for a wide range and higher temperatures. For the entire temperature range considered for the investigation, the 1D simulation results are in good agreement with the reference 2D simulations and experiments. As shown in the figure, the reference data is available only for the methane conversion, however, we have also shown water conversion for the given temperature range for our simulation set-up.

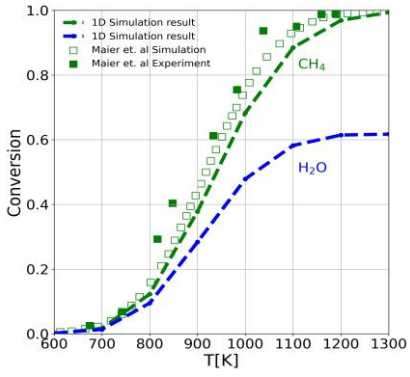

Figure 7: Methane and water conversion as a function of temperature for S/C=3, P=1 atm, $\dot{f}$=593 mL/min and 75% Argon dilution along with the reference data.

Next, the mole fraction for different species (CH_4, H_2O, CO_2, CO, H_2) as a function of temperature is depicted in Figure 8. Here we do not have any reference data to compare with and hence, the results are shown only for the 1D simulations. The simulations are performed for the same conditions as presented for the previous figure, i.e., for Tϵ[600,1300] K and S/C=3. Initially, there is methane and water and all other species are absent. Then with the increase in temperature, methane and water is being consumed and tends to go towards zero whereas, all other species are being formed with increasing temperature. Also, as expected, we find the formation of H_2 is higher with consumption of reactants as compared to the other species, such as, CO_2 and CO.

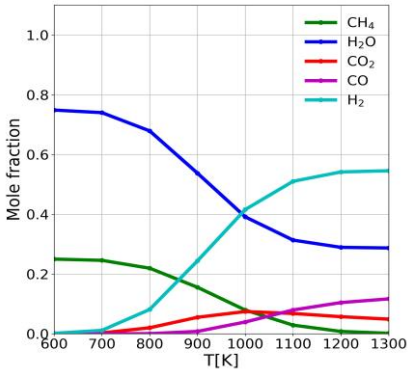

Figure 8: Mole fraction as a function of temperature for S/C=3, P=1 atm, $\dot{f}$=593 mL/min and 75% Argon dilution.

5.2 Variation of S/C Ratio

Here, the variation of some of the above discussed quantities (conversion, selectivity and mole fraction) is shown with changing S/C ratio. The simulations are performed for 3 different S/C ratios as S/C=1.9,2.77 and 3.67. All the other physical and numerical parameters are kept fixed. The simulations are performed for constant temperature as 1020 K, pressure as 1 atm, flow rate as 593 mL/min and 75% Argon dilution. The reference data from 2D simulations and experimental measurements are also plotted for some of the cases.

Figure 9 displays the methane and water conversion as a function of S/C (inlet steam-to-carbon) ratio. The 1D simulation results are in very good agreement with the reference data which illustrates the capability of the model to capture the chemistry correctly. The 1D result shows that the methane conversion increases and the water conversion decreases with increasing S/C ratio. This is in accordance to the reference 2D simulation and experimental results. For the given temperature, the methane conversion is approximately 80% for S/C=2 and increases to ≈97% for S/C=3.77. The methane conversion at medium temperature was observed in the range of 75-55% similar to the literature [24]. At the same time, the water conversion reduces from ≈60% at S/C=2 to ≈40% at S/C=3.77.

International Journal of Environmental Sciences
ISSN 2519-5549 (online)
Vol.5, Issue 1, No.1. pp 1 - 32, 2022
www.iprjb.org

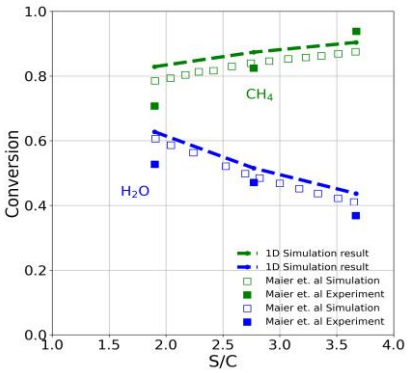

Figure 9: Methane and water conversion as a function of S/C ratio while keeping all the other parameters constant as T=1020 K, P=1 atm, $\dot{f}$=593 mL/min and 75% Argon dilution along with the reference data.

In order to analyze the product composition, the thermodynamic equilibrium in the reaction needs to be considered. So, the CO selectivity is depicted in Figure 10 as a function of the S/C ratio in methane steam reforming for T=1020 K and 75% Argon dilution along with the results from [24]. As expected, the CO selectivity decreases with increasing S/C ratio and varies in between ≈42-37% for S/C=2.0-3.77, respectively. The 1D results are slightly under-predicted as compared to the reference data for low S/C ratio, i.e., for S/C=1.77. Nonetheless, for S/C=2.77, the results are in very good agreement with [24].

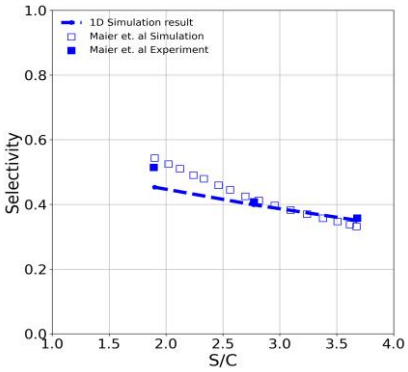

Figure 10: CO Selectivity variation with S/C ratio in methane steam reforming while keeping all the other parameters constant as T=1020 K, P=1 atm, $\dot{f}$=593 mL/min and 75% Argon dilution along with the reference data.

Figure 11 shows the concentration of methane along the reactor length for two S/C ratios, i.e., (a) S/C=1.9 and (b) S/C=3.67 at T=1020 K, P=1 atm and $\dot{f}$=593 mL/min. The methane concentration is noted as independent of S/C ratio. Nevertheless, the initial changes are well captured in the beginning of the simulation and later (t≥2s), there are no changes seen. The simulations are carried out up to 10s only to insure that the steady state is reached.

International Journal of Environmental Sciences
ISSN 2519-5549 (online)
Vol.5, Issue 1, No.1. pp 1 - 32, 2022
www.iprjb.org

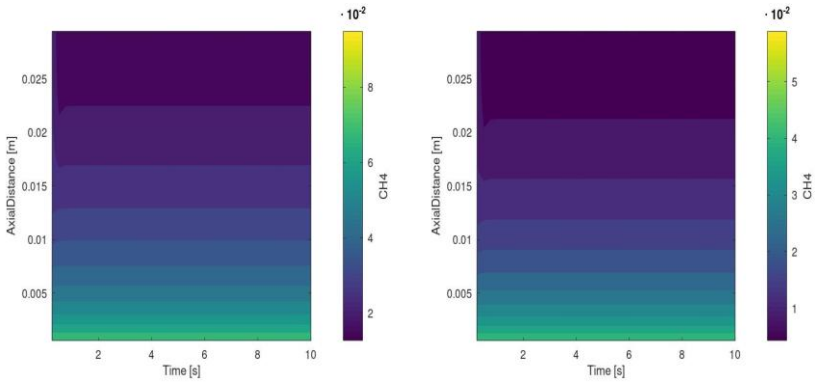

Figure 11: Methane concentration along the reactor for (a) S/C=1.9 and (b) S/C=3.67 at T=1020 K.

5.3 Variation of Flow Rate

Next, the flow rate is varied and different quantities are analyzed in this section. We do not have reference data for this parameter and hence only 1D simulation results are shown and discussed. The simulations are performed with 75% Argon dilution, T=1020 K, S/C=2.77 and P=1 atm as fixed values. Only the flow rate is varied and the results are shown for 3 different flow rates as $\dot{f}$=296,593 and 1186 mL/min.

In Figure 12, the methane and water conversion as a function of flow rate is shown. The other parameters (T, P, S/C ratio) remain fixed. Both the reactants, methane as well as water, show similar trends for the conversion which is reduction with the increasing flow rate. The conversion of methane reduces from ≈ 96% to 77% for $\dot{f}$=296 and 1186 mL/min, respectively and for water from ≈ 57% to 44% for these flow rates. The behaviour is as expected. The investigated catalyst seems to be designed for the initial flow rate.

For visualization, the methane concentration along the reactor length with respect to time is shown in Figure 13. The figure displays methane concentration contours for (a) $\dot{f}$=296 and (b) $\dot{f}$=1186 mL/min, keeping all other parameters as constant. The behaviour reported in the earlier sections is confirmed for this parameter as well.

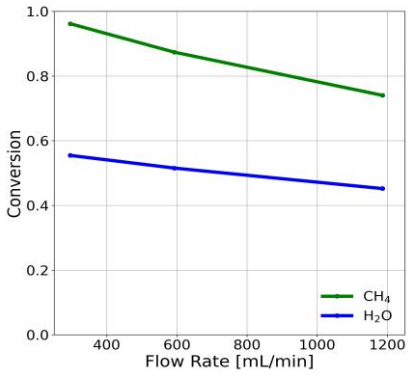

Figure 12: Methane and water conversion as a function of flow rate for T=1020 K, S/C=2.77 and P=1 atm as fixed values and 75% Ar dilution.

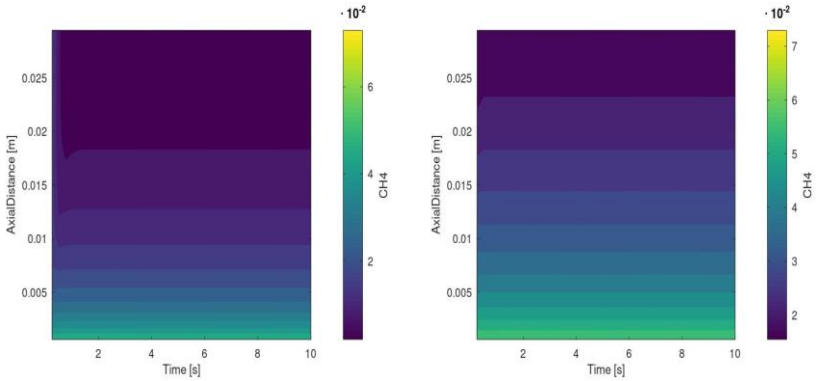

Figure 13: Methane concentration along the reactor for (a) $\dot{f}$=296 and (b) $\dot{f}$=1186 mL/min at T=1020 K.

5.4 Variation of Pressure

In this section, the various quantities are discussed with the variation of pressure keeping the S/C ratio fixed to 3. A wide temperature range is considered for the simulations. The results are presented at 3 different pressures, i.e., 1,10 and 100 atm. It is important to analyse few quantities at higher pressures because for some processes, higher pressures are needed to separate the hydrogen from the methane and recycle the methane to obtain a high purity hydrogen stream [40]. Note that we do not have any reference data for the comparison and hence, our analysis is limited for 1D simulation results.

In Figure 14, the methane and water conversion as a function of temperature is shown for S/C=3 at 3 different pressures. We report that the methane for the low pressure, i.e., at 1 atm is fully converted into the products for the highest investigated temperature. The conversion varies from zero at low temperature, i.e., T=600 K and it reaches to one, i.e., full conversion for T=1300 K. However, as the pressure increases from 1 atm to 10 atm and further to 100 atm, the conversion of methane becomes slower and at the given conditions even at higher temperatures methane is not fully converted into the products anymore. A similar qualitative behaviour is noted for the water conversion.

International Journal of Environmental Sciences
ISSN 2519-5549 (online)
Vol.5, Issue 1, No.1. pp 1 - 32, 2022
www.iprjb.org

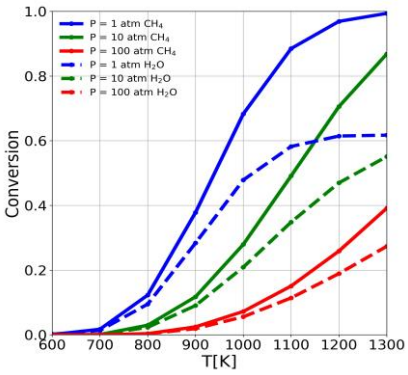

Figure 14: Methane and water conversion as a function of temperature with S/C=3 for different pressures.

Figure 15 illustrates the variation of methane concentration along the reactor length for (a) P=1 and (b) P=100 atm at T=1020 K. As discussed in the previous sections, the major changes in the concentration happen initially, i.e., ≤2s and for t≥2s, the steady state has already reached and no changes are observed. Here, we also attempt to show the behaviour with changing pressure and note that the thermal equilibrium for higher pressure is attained with some delays as compared to the lower pressure.

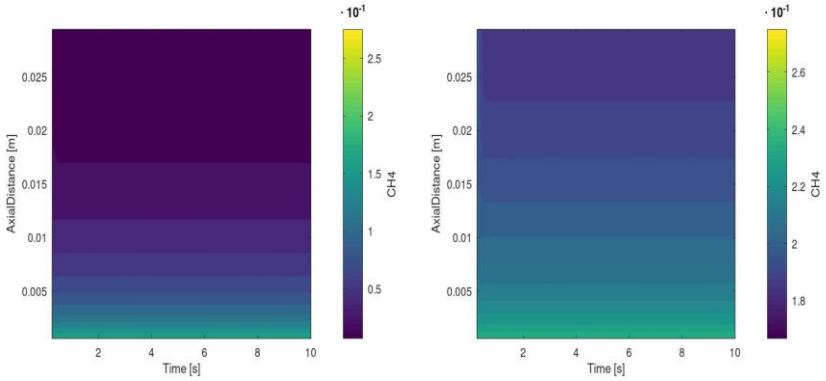

Figure 15: Methane concentration along the reactor for (a) P=1 and (b) P=100 atm at T=1020 K.

6.0 CONCLUSIONS

In this paper, we have presented the kinetics of the steam reforming of methane over nickel catalyst using a one-dimensional tool, LOGEcat. The results are compared with literature [24] and the investigation is carried out for several parameters, for example, temperature, pressure, flow rate and S/C ratio. Various quantities, such as, conversion, selectivity and mole fraction have been discussed.

- The results show that the conversion, selectivity and H_2/CO ratio for temperatures ϵ [920,1020,1120,1220] K are in very good agreement with the reference data considered. The study was further extended for a wide range of temperatures and the 1D simulation results fit very well with [24]. We have additionally provided the variation of mole fraction with temperature for the 1D model.

- However, the over-prediction of the H_2/CO ratio for simulation results in comparison to the experimental measurements at the S/C ratio 2.77 might be due to the underestimation of water-gas shift reaction at low temperature. We plan to further investigate the chemical mechanism within a comprehensive chemical training.
- Likewise, the conversion and selectivity profiles are also given for varying S/C ratio. The model gives matching profiles with the reference 2D simulations and experimental data from [24] for both the profiles.
- Additionally, the conversion profile is shown for varying pressure ($P\epsilon$[1,10,100] atm) and flow rate ($\dot{f}\epsilon$[296,593,1186] mL/min). We do not have reference data for these parameters.
- For visualization, we have also given the reactants and products concentration along the reactor length with respect to time for a fixed temperature and only the methane concentration for all the other parameters (S/C ratio, pressure and flow rate).

The analyses carried out in this paper illustrate the predictive capability of the 1D model. The 1D tool captures the flow physics and chemistry very well for the parameters discussed and is cost effective (numerically fast).

This study recommends further investigations for the reaction mechanism towards the kinetically limited conditions where the catalyst kinetics and internal transport are critical for the simulations. We also propose to analyze the thermochemistry of the species to develop a kinetically consistent reaction mechanism.

REFERENCES

[1] LOGEsoft, 2008. v1.10 www.logesoft.com.

[2] L. M. Aparicio. Transient Isotopic Studies and Microkinetic Modeling of Methane Reforming over Nickel Catalysts. *Journal of Catalysis.*, 165:262– 274, 1997.

[3] J. Aslanjan, C. Klauer, C. Perlman, V. Günther, and F. Mauss. *In: SAE International, Simulation of a Three-Way Catalyst Using Transient Single and Multi-Channel Models.* ISSN: 0148-7191, 2017-01-0966, 2017.

[4] C. H. Bartholomew. Carbon deposition in steam reforming and methanation. *Catalysis Reviews.*, 24:67–112, 1982.

[5] H. S. Bengaard, J. K. Nørskov, J. Sehested, B. S. Clausen, and L. P. Nielsen. Steam Reforming and Graphite Formation on Ni Catalysts. *Journal of Catalysis.*, 209:365–384, 2002.

[6] E. A. Blekkan, R. Myrstad, O. Olsvik, and O. A. Rokstad. Characterization of tars and coke formed during the pyrolysis of methane in a tubular reactor. *Carbon.*, 30:665–673, 1992.

[7] M. C. J. Bradford and M. A. Vannice. Catalytic reforming of methane with carbon dioxide over nickel catalysts II. Reaction kinetics. *Applied Catalysis A: General.*, 142:97–122, 1996.

[8] D. Chen, R. Lodeng, A. Anundskas, O. Olsvik, and A. Holmen. Deactivation during carbon dioxide reforming of methane over ni catalyst: Microkinetic analysis. *Chemical Engineering Science.*, 56:1371–1379, 2001.

[9] V. R. Choudhary, A. M. Rajput, and V. H. Rane. Low temperature oxidative conversion of methane to synthesis gas over Co/rare earth oxide catalysts. *Catalysis Letters.*, 16:269–272, 1992.

[10] K. H. Delgado, L. Maier, S. Tischer, A. Zellner, H. Stotz, and O. Deutschmann. Surface Reaction Kinetics of Steam- and CO_2Reforming as Well as Oxidation of Methane over Nickel-Based Catalysts. *Catalysts.*, 5:871–904, 2015.

[11] O. Deutschmann and L. Schmidt. Modeling the partial oxidation of methane in a short-contact-time reactor. *American Institute of Chemical Engineers AIChE.*, 44:2465–2477, 1998.

[12] D. Dissanayake, M. P. Rosynek, K. C. C. Kharas, and J. H. Lunsford. Partial Oxidation of Methane to Carbon Monoxide and Hydrogen over a Ni/Al2O3 Catalyst. *Catalysis Today.*, 132:117–127, 1991.

[13] B. C. Enger, R. Lødeng, and A. Holmen. A Review of Catalytic Partial Oxidation of Methane to Synthesis Gas with Emphasis on Reaction Mechanisms over Transition Metal Catalysts. *Applied Catalysis A: General.*, 346:1–27, 2008.

[14] K. Fröjd and F. Mauss. A Three-Parameter Transient 1D Catalyst Model. *SAE International Journal of Engines.*, 4 (1):1747–1763, 2011.

[15] A. M. Gadalla and M. E. Sommer. Carbon dioxide reforming of methane on nickel catalysts. *Chemical Engineering Science.*, 44:2825–2829, 1989.

[16] J. M. Ginsburg, J. Pina, T. El Solh, and H. I. de Lasa. Coke formation over a nickel catalyst under methane dry reforming conditions: Thermodynamic and kinetic models. *Industrial & Engineering Chemistry Research.*, 44:4846–4854, 2005.

[17] J. Guo, H. Lou, and X. M. Zheng. The deposition of coke from methane on a NiMgAl2O4 catalyst. *Carbon.*, 45:1314–1321, 2007.

[18] S. Hannemann, J. D. Grunwaldt, N. van Vegten, A. Baiker, P. Boye, and C. G. Schroer. Distinct Spatial Changes of the Catalyst Structure inside a Fixed-Bed Microreactor during the Partial Oxidation of Methane over Rh/Al2O3. *Catalysis Today.*, 126:54, 2007.

[19] D. A. Hickman and L. D. Schmidt. Steps in CH4 oxidation on Pt and Rh surfaces: High-temperature reactor simulations. *American Institute of Chemical Engineers AIChE.*, 39:1164–1177, 1993.

[20] D. L. Hoang, S. H. Chan, and O. L. Ding. Kinetic and modeling study of methane steam reforming over sulfide nickel catalyst on a gamma alumina support. *Chemical Engineering Journal.*, 112(1-3):1–11, 2005.

[21] F. Incopera, D. DeWitt, T. Bergman, and S. Lavine. Fundamentals of Heat and Mass Transfer 6E. 2006.

[22] M. Levent, D. J. Gunn, and M. A. El Bousiffi. Production of hydrogenrich gases from steam reforming of methane in an automatic catalytic microreactor. *International Journal of Hydrogen.*, 28:945, 2003.

[23] Z. W. Liu, H. S. Roh, and K. W. Jun. Important factors on carbon dioxide reforming of methane over nickel-based catalysts. *Journal of Industrial and Engineering Chemistry.*, 9:753–761, 2003.

[24] L. Maier, B. Schädel, K. H. Delgado, S. Tischer, and O. Deutschmann. Steam Reforming of Methane Over Nickel: Development of a Multi-Step Surface Reaction Mechanism. *Topics in Catalysis.*, 54:845–858, 2011.

[25] A. B. Mhadeshwar and D. G. J. Vlachos. Hierarchical Multiscale Mechanism Development for Methane Partial Oxidation and Reforming and for Thermal Decomposition of Oxygenates on Rh. *The Journal of Physical Chemistry: B.*, 109(35):16819–16835, 2005.

[26] B. C. Michael, A. Donazzi, and L. D. Schmidt. Effects of H2O and CO2 addition in catalytic partial oxidation of methane on Rh. *Journal of Catalysis.*, 265:117–129, 2009.

[27] K. Müller, F. Rachow, V. Günther, and D. Schmeisser. Methanation of Coke Oven Gas with Nickel-based Catalysts. *International Journal of Environmental Science.*, 4:73–79, 2019.

[28] R. Quiceno, O. Deutschmann, J. Warnatz, and J. Pérez-Ramírez. Modelling of the high-temperature catalytic partial oxidation of methane over platinum gauze. Detailed gas-phase and surface chemistries coupled with 3D flow field simulations. *Applied Catalysis A.*, 303:166–176, 2006.

[29] Rakhi, V. Günther, J. Richter, and F. Mauss. *In: 63rd International Conference of Scandinavian Simulation Society, Steam reforming of methane over a nickel-based catalyst*. (Abstract accepted), 2022.

[30] K. Ramanathan, V. Balakotaiah, and D. West. Light-off criterion and transient analysis of catalytic monoliths. *Chemical Engineering Science.*, 58:1381–1405, 2003.

[31] J. R. H. Ross, A. N. J. vanKeulen, M. E. S. Hegarty, and K. Seshan. The catalytic conversion of natural gas to useful products. *Catalysis Today.*, 30:193–199, 1996.

[32] J. R. Rostrup-Nielsen. Activity of Nickel Catalysts for Steam Reforming of Hydrocarbons. *Journal of Catalysis.*, 31:173–199, 1973.

[33] J. R. Rostrup-Nielsen. *In: Anderson JR, Boudart M (eds) Catalytic steam reforming in catalysis—science and technology*, volume 5. Springer-Verlag, Berlin/Heidelberg, Germany, 1984.

[34] J. R. Rostrup-Nielsen. Sulfur-passivated nickel-catalysts for carbon-free steam reforming of methane. *Journal of Catalysis.*, 85:31–43, 1984.

[35] J. R. Rostrup-Nielsen and J. H. B. Hansen. CO2-Reforming of Methane over Transition Metals. *Journal of Catalysis.*, 144:38–49, 1993.

[36] H. Santos and M. Costa. Modelling transport phenomena and chemical reactions in automotive three-way catalytic converters. *Chemical Engineering Journal.*, 148:173–183, 2009.

[37] B. T. Schädel, M. Duisberg, and O. Deutschmann. Steam reforming of methane, ethane, propane, butane, and natural gas over a rhodium-based catalyst. *Catalysis Today.*, 142:42–51, 2009.

[38] D. Schmider, L. Maier, and O. Deutschmann. Reaction Kinetics of CO and CO2 Methanation over nickel. *Engineering Chemistry Research.*, 60:5792–5805, 2021.

[39] R. Schwiedernoch, S. Tischer, C. Correa, and O. Deutschmann. Experimental and Numerical Study of the Transient Behavior of a Catalytic Partial Oxidation Monolith. *Chemical Engineering Science.*, 58(3):633– 642, 2003.

[40] M. Steinberg. *The Hy-C Process (Thermal Decomposition of Natural Gas:) Potentially the Lowest Cost Source of Hydrogen with the Least CO_2 Emission*. Upton, N.Y., BNL 61364, Brookhaven National Laboratory, December 1994.

[41] S. Tischer and O. Deutschmann. Recent advances in numerical modeling of catalytic monolith reactors. *Catalysis Today.*, 105:407–413, 2005.

[42] D. L. Trimm. Formation and removal of coke from nickel-catalyst. *Catalysis Reviews - Science and Engineering.*, 16:155–189, 1977.

[43] D. L. Trimm. Coke formation and minimisation during steam reforming reactions. *Catalysis Today.*, 37:233–238, 1997.

[44] W. J. M. Vermeiren, E. Blomsma, and P. A. Jacobs. Catalytic and thermodynamic approach of the oxyreforming reaction of methane. *Catalysis Today.*, 13:427–436, 1992.

[45] S. Wang and G. Q. M. Lu. CO_2 reforming of methane on Ni catalysts: Effects of the support phase and preparation technique. *Applied Catalysis B.*, 16:269–277, 1998.

[46] J. Wei and E. Iglesia. Isotopic and kinetic assessment of the mechanism of reactions of CH4 with CO2 or H2O to form synthesis gas and carbon on nickel catalysts. *Journal of Catalysis.*, 224:370–383, 2004.

[47] J. Xu and G. F. Froment. Methane steam reforming, methanation and water-gas shift: I. Intrinsic kinetics. *American Institute of Chemical Engineers AIChE.*, 35:88–96, 1989.

List of Abbreviations

CH_4	Methane
CO_2	Carbon Dioxide
H_2	Hydrogen
NO_x	Nitrogen Oxides
O_2	Oxygen
H_2O	Water
1D	One-Dimensional
CO	Carbon Monoxide
DOC	Diesel Oxidation Catalysts
Ni	Nickel
NSR	NO_x Storage and Reduction
PSR	Perfectly Stirred Reactor
S	Selectivity
S/C	Steam-to-Carbon
C/S	Carbon-to- Steam
SCR	Selective Catalytic Reduction
TWC	Three-Way Catalyst

Nomenclature

β_r	temperature exponent [-]
Δt	time step [s]
Δx	cell length [m]
Γ_n^0	standard-state surface site density of site type n [mol/m^2]
γ_r	sticking coefficient [-]
Γ_{tot}	total surface site concentration summed over all surface phases [mol/m^3]
$\nu_{i,r}$	stoichiometric coefficients for reaction r and species i [-]
$\nu_{r,i}$	reaction order for the species i [-]
$\dot{f}$	Flow rate [mL/min]
X_i	conversion for species i [-]
x	mole fraction of the species [-]
y_i	mass fraction of species i [-]
A	cross-sectional channel area [m^2]
A_m	catalytic surface area in the current cell [m^2]
$a_{i,n}$	bulk activity for bulk species [-]
A_r	pre-exponential factor [cm,mol,s]
c_p	specific heat capacity at constant pressure [J/kgK]
$C_{i,g}$	concentration of species i in the bulk gas [mol/m^3]
$C_{i,p}$	concentration of species i in the pore layer [mol/m^3]
$c_{p,p}$	specific heat capacity in the pore volume layer at constant pressure [J/mol/K]

$c_{p,s}$ specific heat capacity of the solid material at constant pressure [J/mol/K]
d_h hydraulic diameter of the channel [m]
D_i diffusion coefficient of species i [m^2/s]
D_T thermal diffusion coefficient [m^2/s]
E_r activation energy [kJ/mol]
f_F friction factor [-]
H enthalpy [J/mol]
h_q bulk gas specific enthalpy [J/kg]
h_T convective heat transfer coefficient between bulk gas and surface [W/m^2K]
h_{in} specific enthalpy of the gas from the upstream cell [J/mol]
$h_{j,g\leftrightarrow p}$ specific enthalpy of species j transported between the bulk gas and the pore layer [J/kg]
K_e tunning parameter for the overall reaction efficiency [-]
k_g thermal conductivity of the gas [W/mK]
K_h tunable parameter for the overall heat transfer [-]
K_m tunable parameter for the overall mass transfer [-]
$k_{b,r}$ reverse rate constants [-]
$K_{c,r}$ equilibrium constant given in concentration units [mol/m^3]
$k_{f,r}$ forward rate constant [-]
$k_{m,i}$ conservation mass transfer coefficient of species i [-]
$K_{p,r}$ equilibrium constants in pressure units [-]
$k_{s,l}$ thermal conductivity of washcoat layer l [W/mK]
m sum of all the stoichiometric coefficients of reactants that are surface species [-]
N_{surf} number of different surface materials present in the catalytic converter [-]
$Nu_{T,\infty}$ asymptotic Nusselt numbers [-]
P geometric wetted perimeter of the channel [m]
P_{atm} pressure of 1 atm [atm]
Pr Prandtl number [-]
R_0 universal gas constant [kJ/mol]
S entropy [J/mol/K]
Sc_i Schmidt number for species i [-]

Sh_i Sherwood numbers [-]

$Sh_{T,\infty}$ asymptotic Sherwood numbers [-]

t time [s]

T_g bulk gas temperature [K]

T_w pore layer temperature [K]

v fluid velocity along the channel [m/s]

V_g gas volume in the current cell [m^3]

V_s volume of the solid wall material (washcoat and substrate) in the current cell [m^3]

$V_{p,l}$ gas volume of the pore volume layer in washcoat layer l in the current cell [m^3]

W_k molecular weight of the gas-phase species [-]

$W_{l+1,l}$ radial distance through the washcoat [m]

$Y_{i,g}$ mass fraction of species i [-]

$Z_{i,n}$ surface site fractions for surface species [-]

μ_i dynamic viscosity of species i [kg/ms]

$\omega_{i,g}$ species source term for gas phase reaction [mol/m^3]

$\omega_{i,n}$ species source term from reactions at site n [mol/m^2]

$\omega_{i,p,l}$ species source term for gas phase reactions in the pore layer in washcoat layer l [mol/m^3]

$\sigma_{i,n}$ site occupancy number of species i at site n [-]

τ_n site density of surface phase n [mol/m^2]

$\theta_{i,n}$ site fraction of species i at site n [-]

Nu Nusselt numbers [-]

P Pressure [atm]

T Temperature [K]

Subscript

b reverse

f forward

g bulk gas

i species

in inlet to the cell

l current washcoat layer *p* gas in the pore layer

r reaction

s substrate material